



A Self-Powered Piezoelectric Nanofibrous Membrane as Wearable Tactile Sensor for Human Body Motion Monitoring and Recognition

Jingcheng Li¹ · Jing Yin^{1,2} · Mei Gui Vanessa Wee^{1,3} · Amutha Chinnappan¹ · Seeram Ramakrishna¹

Received: 13 January 2023 / Accepted: 16 March 2023 / Published online: 11 April 2023
© Donghua University, Shanghai, China 2023

Abstract

Wearable sensors have drawn vast interest for their convenience to be worn on body to monitor and track body movements or exercise activities in real time. However, wearable electronics rely on powering systems to function. Herein, a self-powered, porous, flexible, hydrophobic and breathable nanofibrous membrane based on electrospun polyvinylidene fluoride (PVDF) nanofiber has been developed as a tactile sensor with low-cost and simple fabrication for human body motion detection and recognition. Specifically, effects of multi-walled carbon nanotubes (CNT) and barium titanate (BTO) as additives to the fiber morphology as well as mechanical and dielectric properties of the piezoelectric nanofiber membrane were investigated. The fabricated BTO@PVDF piezoelectric nanogenerator (PENG) exhibits the high β -phase content and best overall electrical performances, thus selected for the flexible sensing device assembly. Meanwhile, the nanofibrous membrane demonstrated robust tactile sensing performance that the device exhibits durability over 12,000 loading test cycles, holds a fast response time of 82.7 ms, responds to a wide pressure range of 0–5 bar and shows a high relative sensitivity, especially in the small force range of 11.6 V/bar upon pressure applied perpendicular to the surface. Furthermore, when attached on human body, its unique fibrous and flexible structure offers the tactile sensor to present as a health care monitor in a self-powered manner by translating motions of different movements to electrical signals with various patterns or sequences.

Keywords Electrospinning · Nanofiber · Piezoelectric sensor · PENG · Wearable · Self-powered device

Introduction

Transitioning towards an intelligent society, digitalization has been reforming the ways people interacting with others rapidly. Traditional means of monitoring and tracking human motion are being replaced with more efficient, sustainable and smart approaches that wearable and flexible electronics came into increasingly significant roles [1–3]. Recovered from the COVID-19 pandemic, the increasing

awareness of health monitoring among public has led to an unprecedented need for high performance wearable electronics capable of detecting vital physiological signals or monitor physical activities in real time. These wearable electronics are expected to exhibit flexibility, lightness, ease of adhesion to human skin, and withstand mechanical deformation to provide the necessary comfort and avoid disturbing regular activities [4, 5]. Wearable sensors can help tracking user's health data such as vital signals or user's activities and thereby improving the quality of life. A variety of applications have been reported including movement tracking recognition, rehabilitation, intelligent sports, biosignal tracking, and other healthcare applications [6–10].

Among the various forms of wearable sensors, self-powered sensors have been receiving vast attention due to their inherent material features, which enable them to operate multifunctionally and independently of external power sources [11–13]. These standalone-operatable devices are particularly appealing as they are free from the limitations of bulkiness of power units and are renewable, sustainable, and portable. Additionally, promoting self-powered electronics

✉ Seeram Ramakrishna
seeram@nus.edu.sg

¹ Centre for Nanotechnology and Sustainability, Department of Mechanical Engineering, National University of Singapore, Singapore 117081, Singapore

² National Engineering Laboratory for Modern Silk, College of Textile and Clothing Engineering, Soochow University, Suzhou, China

³ Integrative Sciences and Engineering Program, NUS Graduate School, National University of Singapore, Singapore 119077, Singapore

presents a potential solution for alleviating energy supply burdens and facilitating sustainable development pathways. The self-powering mechanisms commonly employed for wearable sensors by energy harvesting can be categorized as triboelectric, piezoelectric, thermoelectric and pyroelectric, where piezoelectric nanogenerators (PENG) have shown great potential and ability to respond to tactile stimuli with high mechanical-to-electrical conversion efficiency as a result of their stable responsiveness [14–16].

Materials exhibit piezoelectric properties have been widely investigated since their discovery. Among them, polyvinylidene fluoride (PVDF) and its copolymers have emerged as popular piezoelectric polymers owing to their excellent piezoelectric (PE) performance and superior chemical, mechanical, and thermal properties [17, 18]. PVDF-based nanofibers have found widespread use in tactile sensing applications thanks to their ultra-sensitivity, high flexibility, good chemical resistance, low permittivity, and outstanding thermal stability, which are particularly suitable for wearables [19]. For instance, PVDF-based sensors for pressure sensing [20–22], gait detection [23], acoustic detection [24] and sports monitoring [25] have been developed, leveraging their significant advantages in piezoelectric performance, long-term stability, applicability on curved surfaces, and potential for use in dynamic environments. Furthermore, PVDF exhibits very good biocompatibility and is devoid of any odor, taste, or toxicity, rendering it a highly viable option for wearable devices that come into contact with the skin [26, 27].

It is worth noting that the structure and properties of PVDF can be effectively manipulated through nanoscale fabrication, where the electrospinning process stands out as a one-step, low cost, scalable and versatile process [28, 29]. Despite the crucial roles electrospun nanofibers (ESNFs) have played in fields such as filtration and biomedical scaffolds [30–33], and been employed as substrates in a wide range of applications due to their unique porous structure, air permeability, and large surface to volume ratio [34, 35], the ease of feature modification and attributes design greatly enhances the practicality of employing ESNF membranes as active functional layers for tactile sensing. For instance, incorporating additives such as ZnO nanorods into PVDF ESNFs can boost the power output [36]; introducing unique hierarchical structures such as core-sheath microfibers can bolster their flexibility to withstand intense external deformation [37]; utilizing post-treatment methods including crystallization and poling of fiber membranes can augment their piezoelectric properties [38]. Moreover, the fiber morphology can be tuned by varying parameter combinations, such as solution parameters including viscosity, surface tension, and process variables such as voltage, flow rate, collecting distance, rotating speed of the collector drum, as well as ambient parameters such as humidity and temperature

[19, 39, 40]. In addition, the electrospinning process involves drawing a viscous PVDF solution under a strong electric field, which promotes the formation of PVDF nanofibers with a favorable polar phase transformation, resulting in an increased β -phase content and enhanced piezoelectric properties [11, 28, 41, 42].

Here in this work, we present a self-powered, lightweight, breathable, robust, and efficient flexible tactile sensor fabricated from PVDF-based nanofiber (NF) membranes with low-cost, facile assemble fabrication strategy through electrospinning. We first investigate the impact of multi-walled carbon nanotubes (MWCNTs) and barium titanate (BTO) particles as additives on the mechanical and electrical behaviors of PVDF ESNFs. Mechanical and electrical properties of the ESNF membranes including fiber morphology, tensile strength, hydrophobicity, water permeability, dielectric permittivity and crystallinity are examined. Membranes with optimized parameters and tactile sensing characteristics are employed as a PENG. By assembling the functioning layers, the ESNF based PENG device is capable of sensitively responsive to mechanical stimuli induced deformation, which shows potential for bio-mimical force sensing and human-machine interaction applications with ease of replication and low cost. Besides, benefiting from its outstanding electrical and mechanical properties, the PENG device exhibits a wide working range (0–5 bar), with a stable sensitivity quantified by the generated open circuit voltage (11.6 V/bar below 0.5 bar and 660 mV/bar within the range of 0.5–5 bar) that reaches up to 9.7 V upon pressure. Excellent repeatability and mechanical durability are validated as well. Furthermore, we investigate the role PENG tactile sensor plays in health-caring and exercise monitoring scenarios, including multi-location piezoelectric signal tracking from elbow, hip, thigh, knee and ankle. Overall, the PENG sensors demonstrated great potential for multifunctional monitoring and motion recognition through analysis of the generated waveform signal patterns. With high sensitivity and stable performance, the PENG tactile sensor presents itself as a promising tool for healthcare monitoring in a variety of scenarios and human machine interfaces.

Experimental Section

Nanofibrous Membrane Preparation

For pristine PVDF nanofiber membrane, the electrospinning solution was prepared by dissolving PVDF powder (Sigma-Aldrich, avg. Mw = 192 k) in the solvent of 3:2 (v/v) dimethylformamide (DMF)/Acetone mixture (both from Sigma-Aldrich) with a controlled amount (16 wt%) at 45 °C, followed with continuous magnetic stirring overnight. Solution for electrospinning of CNT/PVDF NF

membrane was prepared by MWCNTs (AP-SWNT, Carbon Solutions Inc) dispersion prior to PVDF mixing. MWCNTs were dispersed in the same solvent mixture along with sodium dodecyl sulfate (SDS) (USB Corporation) to improve its dispersion [43, 44], where the weight ratio of SDS was kept at 0.04%, weight fraction of MWCNT was kept at 0.01%. This mixture was kept for sonication of 180 min to achieve a uniform solution. Then, PVDF powder was added with a controlled amount (16 wt.%) by continuous magnetic stirring overnight at 60 °C to ensure complete dissolve. The obtained composite solution was filled in a plastic syringe with a stainless-steel needle with 0.337 mm inner diameter for the subsequent electrospinning process. The syringe was placed around 15 cm from the grounded rotating collector with a diameter of 30 cm and running at a rotating speed of 200 rpm, where a high voltage of 21 kV supplied from a high voltage power supply was applied on the needle tip via a conductive metal clip. Meanwhile, the solution was fed by a syringe pump at a feed rate of 1 mL/h. Collected nanofiber membrane was dried on a hotplate at 70 °C for 12 h.

A weight fraction of 10% BTO powder (Sigma-Aldrich, particle size < 2 µm) was dispersed in same DMF/acetone solvent mixture by 10 min of sonication. PVDF powder of 16% weight ratio was then dissolved in the solution same way as that for CNT/PVDF solution preparation method. This solution parameter combination is optimized to get the satisfactory morphology for electrospinning as discussed in previous work [45]. Settings for electrospinning of BTO@PVDF nanofiber film are consistent with that of CNT/PVDF nanofiber film except that high voltage power supply used was 22 kV and feed rate was kept at 0.8 mL/h.

Tactile Sensor Device Assembly

The as-spun NF membranes possess great hydrophobicity and air permeability, and biocompatibility of PVDF [26] makes it suitable to directly attach on human skins for piezoelectric effects empowered tactile sensing. For the convenience of characterization of the PE response, we encapsulated the BTO@PVDF NF membrane, which was cut into a 2 × 2 cm square, by sandwiching it between polyethylene terephthalate (PET) films (Innox Higa Singapore pte.ltd.) for protection and adopted Copper tapes (3 M) for connecting electrodes. After exhaustion of air gap between the fibrous membrane and Cu tape, the whole device was sealed with insulation tapes on all sides to make sure there exists no air gap between the electrodes and fiber membrane, nor between the electrode and the protection layer to prevent triboelectric effects from occurring at the contact surface of two different materials. Device assembly sequence is illustrated in Fig. S1.

Characterization

A field emission scanning microscope (FESEM) (JOEL JSM-6701 F) was used to visualize fiber morphology and particle distribution of electrospun nanofibers. A micrometer was used to measure the thickness of nanofiber layers. Mechanical testing was carried out by an Instron Microtester 5500 instrument, testing at a rate of 1 mm per second. Samples for the tensile test were cut into dumbbell shape following ASTM D1708. A LCR meter (KEYSIGHT E4980A) was used to evaluate the dielectric properties of the nanofiber membranes. Measurement was carried out with a bias voltage of 500 mV for frequency range of 20 Hz to 2 MHz. A Bruker D8 Advance diffractometer using Cu K α radiation ($\lambda = 1.5406\text{\AA}$) and Spectrum 2000 FTIR spectroscopy was used to analyze crystalline structure and phase compositions of the as-spun composite nanofibers, with scanning 2θ range of 10° to 80° at 0.02° per second. Output electrical performance of the as-prepared PENG was evaluated by a source meter unit (Keithley 2450). A load test machine (JSV-1000, Measuring Instrument Technology) was applied as the external stimulates which can provide a continuous and periodic load-release motion with controlled levels of displacement. All data acquired were then visualized and analyzed with either python3.8 or Veusz software, except that fiber diameters were measured using ImageJ software for quantification and statistical analysis of nanofibers. More than 100 different measurements obtained over multiple locations of fiber membrane were averaged for each measurement.

Results and Discussion

Electrospun Piezoelectric Nanofiber Membrane

Schematic diagram of the electrospinning process is depicted in Fig. 1a. As shown, a high voltage power supply creates the electric field for solution fed by a syringe pump and pulled out that formed a Taylor cone at the tip of needle, and ejected jets were then solidified on a grounded rotating drum collector. Afterwards, the solidified fibers were collected as nanofiber membrane. Fiber morphology of the obtained fibers from PVDF, PVDF with CNT, and PVDF with BTO solutions and their respective diameter distribution are investigated. Electrospinning processing parameters were optimized to get uniform, continuous, free of beads or drops, random oriented fibers, which possess an overall balanced diameter distribution and can be clearly seen from the SEM images (Fig. 1b, Fig. S2). Due to electrospinning parameters variation, among three PVDF based electrospun nanofibers, CNT/PVDF nanofiber has the largest mean diameter of 745.65 ± 49.5 nm, and BTO@PVDF nanofiber has an average diameter of 436.87 ± 26.8 nm, improved around 29.4%

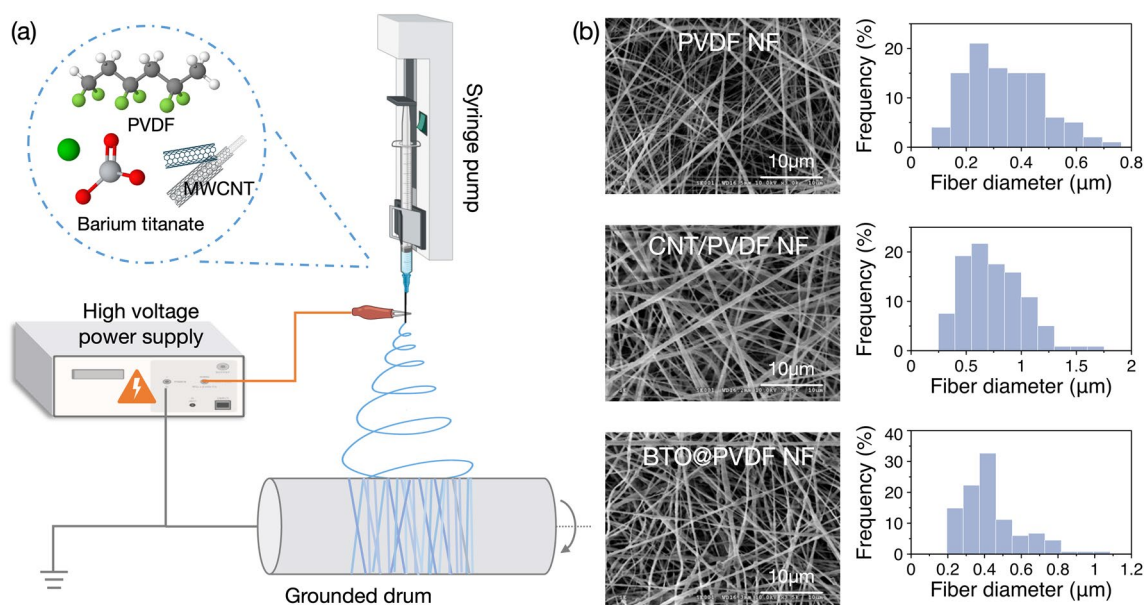


Fig. 1 Preparation of nanofiber membrane. **a** Schematic diagram of the electrospinning process, **b** SEM images of three types of nanofibers and their diameter distribution

compared to pristine PVDF (337.62 ± 27.6 nm) without the addition of BTO particles.

Characteristics of NF Membranes

Mechanical and electrical properties of the ESNF membranes are then investigated. Tensile test results of three types of nanofiber membrane prepared by electrospinning (Table 1) validates the impact of added CNT on improving ESNF's mechanical properties.

Accordant with Table 1, stress-strain curves (Fig. 2a) of these three types of ESNFs help demonstrate that CNT/PVDF NF membranes are with the highest Young's modulus and can bear higher tensile strength, with a price of lower elongation ability when stretching. It is assumed that addition of CNT induces β -phase of the PVDF NF and increases the elasticity [17]. Interestingly, the addition of BTO particles appears to weaken the strength of the ESNF membrane. This is because the size of BTO particles (with a diameter of ~ 1 μm) is bigger than the average diameter of nanofiber (Fig. 1b left bottom), forming a bead-on-string-like structure that disrupts the continuity of nanofibers. However, as can

be seen from the SEM images, introduction of BTO particles along the PVDF fibers increased the surface roughness of the fiber membrane, resulted in more frequent and intense friction as well as bigger contacting area among fibers when pressure applied, thus contributes to improved dielectric property (Fig. 2b) and hydrophobicity (Fig. 2c) of BTO@PVDF NF over pristine PVDF NF.

Consider ESNF membranes equivalent to the dielectric material in a capacitor, so that their dielectric relative permittivity can be calculated by $k = \frac{C}{C_0}$, where C is the capacitance of the membrane, C_0 is the capacitance in the absence of the nanofiber mats which calculated by $C_0 = \frac{\epsilon_0 A}{d}$, where free space permittivity $\epsilon_0 = 8.85 \times 10^{-12}$ F/m, A and d represents the area and thickness of measured sample, respectively. Measurement at each frequency contains at least 3 datapoints. The variation of calculated dielectric constant (k) as a function of frequency for three ESNF membranes is plotted in Fig. 2b. As shown, the k value slightly decreases with increasing frequency due to frequency-dependent interfacial polarization effects [46] but possess overall stability. Also, an

Table 1 Mechanical properties of electrospun nanofiber membranes

Mechanical properties	PVDF NF	CNT/PVDF NF	BTO@PVDF NF
Young's modulus (MPa)	0.29 ± 0.02	0.57 ± 0.09	0.18 ± 0.03
Yield strength (MPa)	0.92 ± 0.17	2.18 ± 0.49	0.43 ± 0.07
Ultimate tensile strength (MPa)	1.72 ± 0.40	2.95 ± 0.50	0.61 ± 0.06
Elongation at break (times)	2.47 ± 0.33	1.49 ± 0.06	0.79 ± 0.03

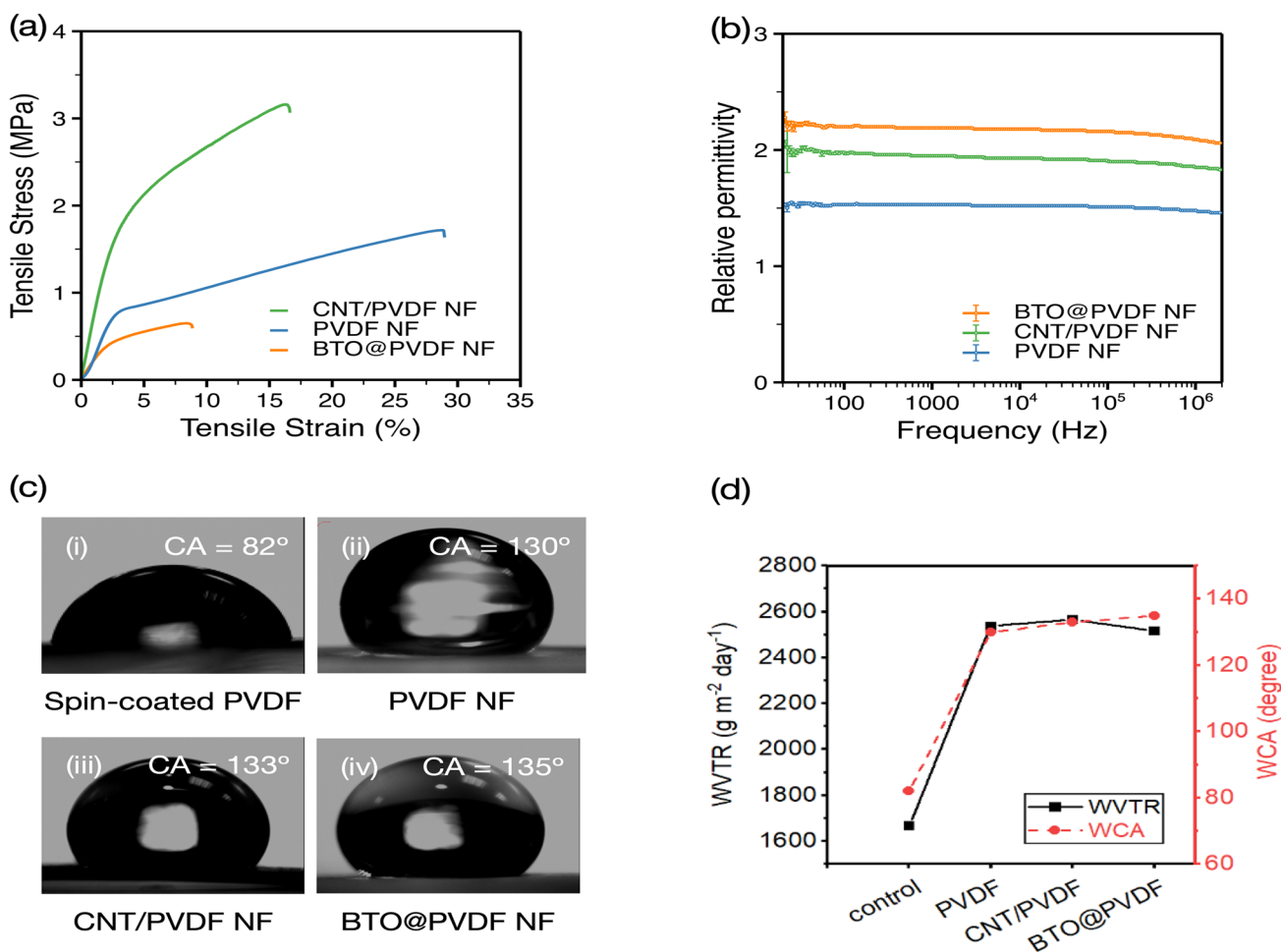


Fig. 2 Characterization of the hydrophobic nanofiber membranes. **a** Tensile test results of nanofibers showing CNT/PVDF nanofiber has the best mechanical property in tensile test, **b** Dielectric spectra result of three ESNF membrane as a function of frequency showing improved dielectric constant with additives to PVDF nanofibers, **c** Water contact angle test results show hydrophilic surface of

spin-coated PVDF film (i) becomes hydrophobic after electrospinning as (ii) PVDF electrospun nanofiber film, this hydrophobicity further increased with additives of CNT (iii) and BTO (iv), **d** Water vapor transmission rate comparison of nanofibers, conducted with bottles filled with water and each covered with nanofiber mat in a closed environment of 37°, RH 60% to let water naturally evaporate

improvement of k value can be observed with the addition of CNT and BTO particles in PVDF ESNFs across all frequency range, which is more prominent in lower frequencies. Increase in k of the PVDF with the addition of CNTs or BTO nanoparticles is due to the poor conductivity of the polymer matrix and great dielectric permittivity difference between the PVDF matrix and the additives, leading to accumulation of charges that can be carried at the interface [47, 48]. For example, addition of BTO particles boosted the dielectric permittivity of PVDF NF improved over 105% at 10 Hz and over 78% on average through all frequencies. Trend of improvement ratio of k with respect to frequency is plotted in Fig. S3. Compared to melt-mixed solid samples, porous PVDF ESNFs have lower dielectric constants because of their different degree

of porosity, especially when high β -phase content induced [49–51]. Similar results were observed in the studies where increased β -phase content in the PVDF leads to decreased dielectric permittivity [52]. That is to say, applications such as energy storage demands high dielectric constant [53], whereas ESNF membrane with an appropriate level of permittivity allows the electrons to transfer freely and at the same time, minimize the electrons stored inside.

A hydrophobic surface of the membrane is desired since it prevents pollution and fouling [54]. Water contact angle tests confirms that process of electrospinning certainly brings outstanding hydrophobicity to the membrane by modifying the surface roughness (Fig. 2c). Spin-coated PVDF exhibits a slightly hydrophilic surface, whereas after electrospinning,

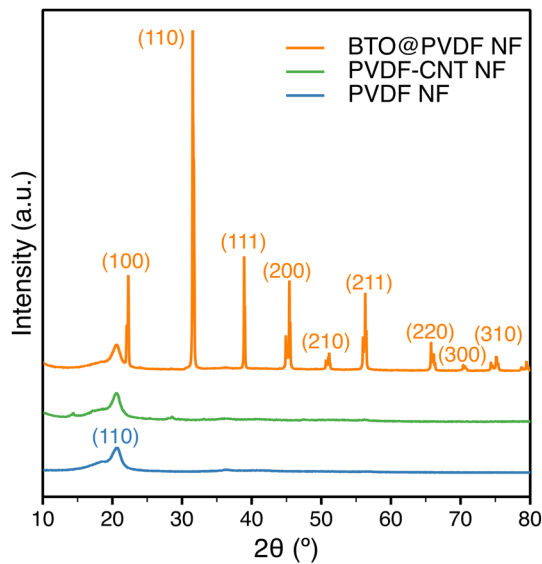


Fig. 3 XRD spectra of three types of ESNF membranes

PVDF ESNFs appears to be hydrophobic with a water contact angle of 130° , which further increases to 133° for CNT/PVDF and 135° for BTO@PVDF membrane. Additionally, all membranes showed good breathability after a 24 h water permeability test measuring the weight loss of vaporized water under 37°C which mimics human body temperature (set up shown in Fig. S4). Water vapor transmission rate (WVTR) is then calculated by $WVTR = \Delta m/A \times t$, where Δm denotes the average mass difference of water of at least three sample groups, A represents the water vapor transmission area, and t represents the time span of the test. As shown in Fig. 2d and Fig. S5, CNT/PVDF membrane exhibits the highest WVTR of $5.429 \text{ kg}\cdot\text{m}^{-2}\cdot\text{day}^{-1}$, presumably due to its larger fiber diameter and pore sizes, while BTO@PVDF has a WVTR of $5.313 \text{ kg}\cdot\text{m}^{-2}\cdot\text{day}^{-1}$ and $5.324 \text{ kg}\cdot\text{m}^{-2}\cdot\text{day}^{-1}$ for pristine PVDF membrane, which are comparable or higher than reported breathable nanofiber membranes [55–57]. As a result, advanced hydrophobicity, breathability, and water permeability demonstrate the possibility of utilizing these

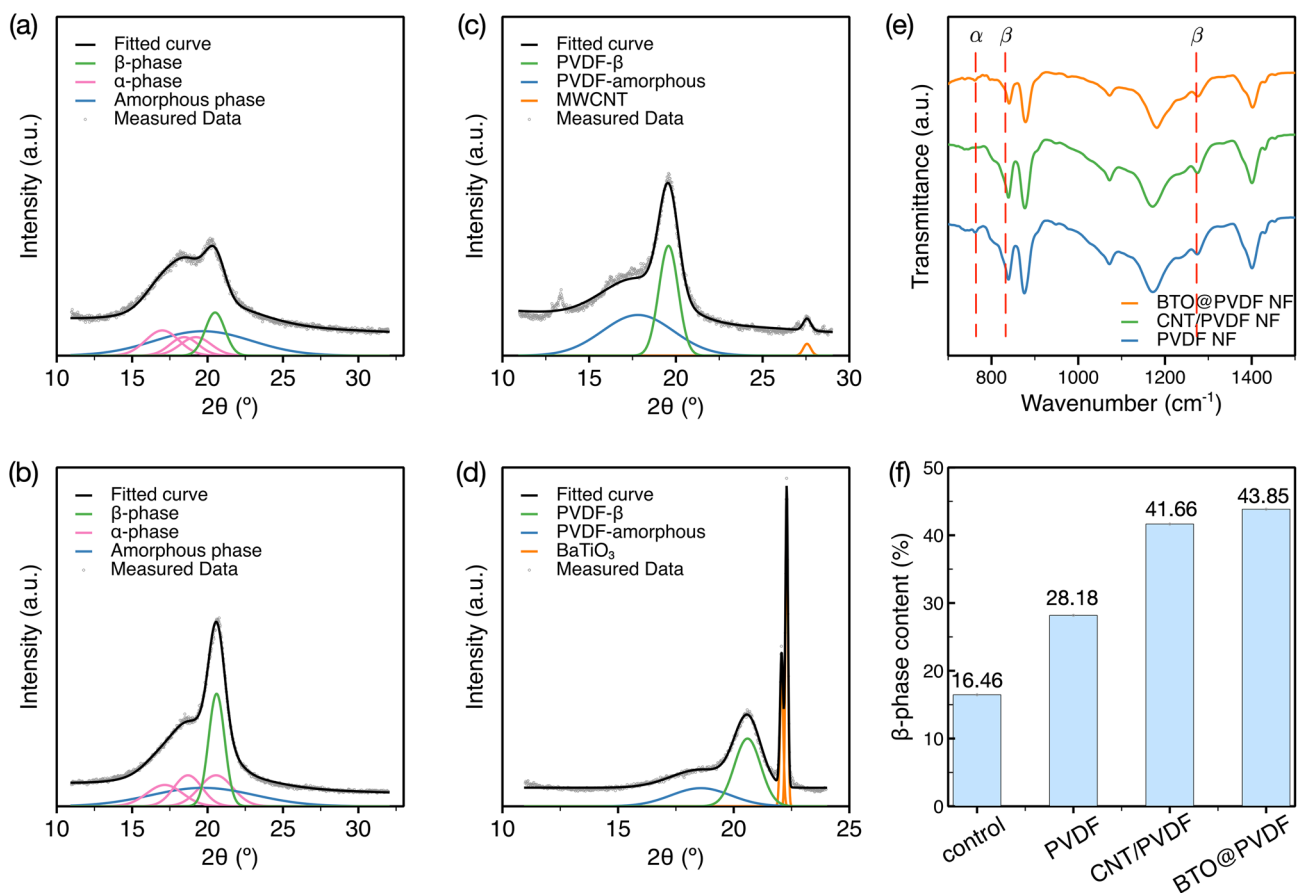


Fig. 4 Improved β -phase content ratio through electrospinning and additives in nanofibers. XRD patterns and corresponding characteristic peaks fitting showing improved β -phase crystalline content of nanofiber membranes prepared by electrospinning compared to spin-coated film from the same solution: **a** spin-coated PVDF, **b** PVDF

nanofiber, **c** CNT/PVDF and **d** BTO@PVDF. **e** FTIR verifies phase contents of electrospun nanofibers from 16 wt% PVDF (blue), CNT/PVDF (green) and BTO@PVDF (orange). **f** β -phase content ratio in percentage over four types of PVDF-based films, where spin-coated PVDF film is the control

ESNF membranes as e-skin substrates or skin-contacted tactile sensors.

Crystalline Phase Analysis

Electrospun PVDF fibers can be semi-crystalline, and their polymorphic behavior and electroactive properties rely on the crystalline phase variation. PVDF β -phase possesses superior piezoelectric and pyroelectric properties because of the well-oriented polarized structure of the all trans planar zigzag conformation [58].

X-ray diffraction (XRD) spectra were used to characterize the crystallinity of PVDF-based membranes. XRD results (Fig. 3, Fig. S6) and their fitted curves (Fig. 4) confirmed the boosted presence of β -phase content.

To analyze the crystallinity of PVDF-based membranes quantitatively, XRD patterns of the spin-coated pristine PVDF, PVDF ESNFs, CNT/PVDF ESNFs, and BTO@PVDF ESNFs were simulated with multipeak fitting and shown in Fig. 4a–d, respectively. Comparing PVDF membranes prepared by electrospinning and spin-coating from the same solution, the notably increased peak intensity at $2\theta = 20.5^\circ$ (Fig. S6, Fig. 4a and b) indicating the pulling effect of electrical force of electrospinning process on β -phase content enhancement [59], which is higher than the intensity at 18° that indicates α -phase conformation. The spin-coated PVDF membrane shows an amorphous phase and diffraction peaks at 17.5° , 18.5° , 19° that correspond to α -phase, and 20.5° for β -phase [11]. It is believed that electrical poling changes the conformation of the phase contents, by which electrospinning played a critical role in promoting inter-chain registration, and not only greatly promotes β -phase formation but also enhances the polarization alignment in the resulting PVDF nanofibers. Further, the fraction of the β -phase is calculated with equation: $F(\beta) = A_\beta / (A_\alpha + A_\beta + A_{amo})$, where $F(\beta)$ is the β -phase content fraction, A_α , A_β and A_{amo} represent the peak area of α -, β - and amorphous phase, respectively [11, 60]. After electrospinning, the dominant α - and γ -phase [61] coexisting with β -phase [62] has changed to an increased β -phase content from 16.46 to 28.18% (Fig. 4f), implying that electrospinning contributes to the formation of β -phase crystallinity in PVDF nanofiber membrane [63]. The results show β -phase fraction of the PVDF nanofibers is significantly enhanced compared with addition of additives that increased to 41.66% with CNT and 43.85% for BTO particles. As shown in Fig. 4c and d, the presence of CNTs and BTO particles helps formation of the β -phase in PVDF [64] and boost the electrical property of the device, as they can be semi-conductive depending upon tube diameter and chirality [65]. During electrospinning of CNTs dispersed PVDF solution, CNTs act as nucleating agents that benefits jet elongation, electro-static reactions act between

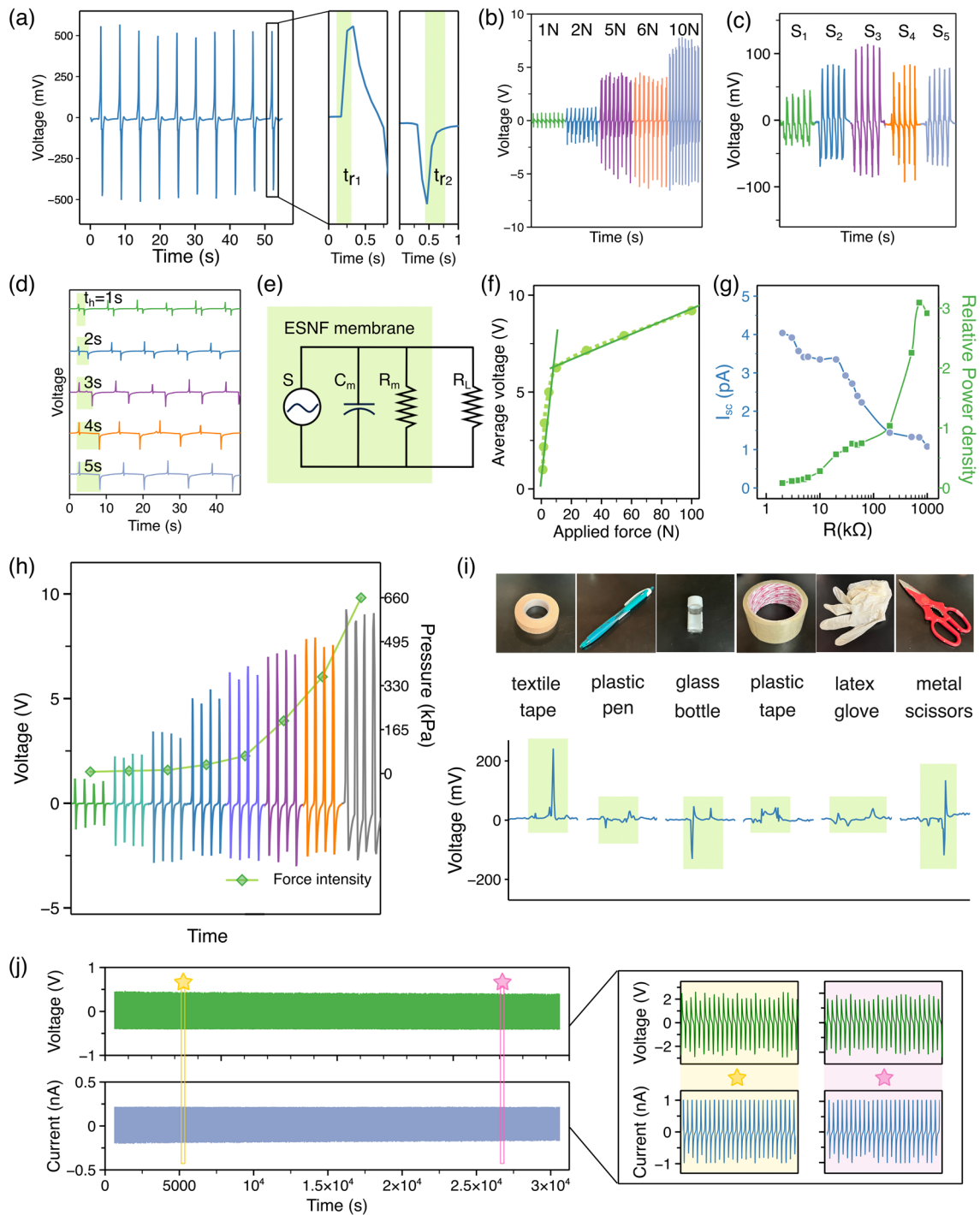
CF_2 groups of PVDF and the functional groups to reach a crystallization ratio [17, 62]. Similarly, BTO particles provides more nucleation sites to form more β -phase in PVDF [66].

Furthermore, Fourier-transform infrared spectroscopy (FT-IR) analysis was performed as well to examine the crystalline contents since several unique characteristic peaks can be represented to identify α -, β - and γ -phases. IR absorption bands of β -phase are located at 840 and 1279 cm^{-1} (Fig. 4e) as strong supporting evidence for the β -phase crystal, yet vibrational bands at 766 , 795 , 976 , 1210 cm^{-1} that deterministic for α -phase are nearly negligible [58, 59, 67]. It can be noted that a tiny peak appears at 1234 cm^{-1} band for γ -phase, which could relate to the relaxation process ($\beta \rightarrow \gamma$) that often occurs in stretched PVDF samples [68].

Tactile Sensing Performance of the PENG

The self-powered sensing device was assembled with NF membrane sandwiched between conductive electrodes and encapsulations (Fig. S1) and works with piezoelectric effects. This PENG device consists of multiple functional layers where the nanofiber membrane serves as active sensing and electron generating layer, copper as conductive layers and PET as protective layers. In the absence of disturbance, the electric dipoles oscillate in a random manner, which happens within a certain tiny range regards to their aligned axes and maintaining a constant overall level of average spontaneous polarization [69, 70]. Mechanical deformation introduced to the PENG's surface will compress the device, and significantly reduce the total spontaneous polarization. Working as a PENG, the tactile sensor is capable of sensitively responsive to mechanical stimuli induced deformation, which shifts the polarity and generates imbalance in electron distribution, in turn to be reflected as electron flow. The inherent concise structure endows it ease to assemble and replicate with low cost and self-powering capability as a nanogenerator saves the device from extensive bulky supporting circuits.

This decrease of induced charges leads to generation of a flow of electrons, which conversely cause an opposite direction of electron flow when the compression is withdrawn and polarization get recovered to its original state [23]. Typical waveform responses upon pressure of the PENG tactile sensor are shown in Fig. 5a, which carried out a fast response time of $t_{r1} = 82.7\text{ ms}$ and an average recover time of $t_{r2} = 248\text{ ms}$. Sensing performance of the PENG were evaluated by applying a series of force with various intensity (Fig. 5b), it can be seen obviously that the output voltage increased with higher pressure implemented. To investigate the effective functional surface area of the PVDF ESNF membranes, various sizes of membrane area are chosen to conduct the loading test. It can be seen in Fig. 5c that upon cyclic load of



0.5 N, membrane with side length 2 cm, area S_3 exhibits the maximum voltage output and thereby chosen for the following applications. This size is also appropriate to be attached on skin to fit the curvature of human body so that the PENG can serve as a wearable sensor, which will be discussed later. Moreover, Fig. 5d shows the voltage response generated with pressure applied which held for a short period (t_h) before release, and t_h was set to 1, 2, 3, 4, and 5 s respectively.

Notably, the waveform shows a lag in-between the positive and negative peaks correspondence with t_h , which identifies the characteristic of piezoelectric response, and assures the identification of tactile sensing pattern from acquired waveform pattern.

The equivalent circuit model was developed for the ESNF membrane-based PENG when viewing it as whole (Fig. 5e). The short-circuit current (I_{sc}) curve with varying resistive

Fig. 5 Waveform spectrum of electrical responses from self-powered nanofibrous PENG. **a** A typical response of the PENG device generating open circuit voltage when periodic pressure applied on contact area of 2 cm^2 under the contact force of 0.8 N every 4 s . Zoomed-in view of the signal waveform showing a fast response time $t_{r1} = 82.7\text{ ms}$, an average recover time $t_{r2} = 248\text{ ms}$, **b** the PENG device shows increased value of voltage when applied with higher intensity of pressure, **c** voltage responses of PENG device under a cyclic load of 0.5 N with various size of the active BTO@PVDF ESNF membranes, the devices are square-shaped with area of S_1 to S_5 , of which the side lengths are controlled to be $1.2, 1.7, 2, 2.5, 3\text{ cm}$, respectively, **d** voltage response of the PENG with applied pressure with a cycle of every 5 s and a short holding before release, where holding period $t_h = 1\text{ s}$ and $2\text{ s}, 3\text{ s}, 4\text{ s}, 5\text{ s}$, respectively, **e** a simplified equivalent circuit of the ESNF based PENG, where S, C_m, R_m denotes the equivalent voltage source, capacitance and resistance of ESNF PENG, respectively, and R_L represents the external load, **f** fitted curve of average voltage amplitude with respect to applied force showing a two-stage sensitivity of the tactile sensor, **g** short circuit current as a function of resistive load and its corresponding relative power density, **h** PENG's generated voltage output versus applied force, **i** PENG's response to various common laboratory objects, **j** the device shows great dynamic durability and performs stability after over $12,000$ pressing-releasing cycles (left). Zoomed-in waveform electric responses (right) of generated open circuit voltage (upper section) and current (lower section)

loads of individually operated PENG was plotted by substituting changing load in the circuit, relative power density was derived accordingly as illustrated in Fig. 5g. With Ohm's law, the current output exhibits exponential descending trend associated with the resistive load, while the calculated peak relative power density was observed with the load of $1\text{ M}\Omega$. In Fig. 5h, voltage output variation against applied force intensity with a wider span was employed to further investigate the sensitivity of the PENG. Subsequently, the relative sensitivity of the tactile sensor can be calculated by finding the slope of fitted Force-Voltage curve. As shown, the sensor exhibits a two-stage sensitivity (Fig. 5f), where in a narrower pressure range of precision within 0.5 bar , a response of 11.6 V/bar is shown. Whereas for stimulus with a wider range of $0.5\text{--}5\text{ bar}$, it performs a less steep slope: a diminished sensitivity of 660 mV/bar , which are comparable or higher than the sensitivity of similar PVDF ESNFs based tactile sensors (Table S1, Fig. S7). As the result, its high sensitivity in minor pressure range makes it an ideal candidate for tactile sensor especially for human motion sensing, capturing subtle mechanical deformation introduced by movements in real time.

Assured the tactile sensing capability of the PENG, a set of common objects found in laboratory were gently placed on the device. As exhibited in Fig. 5i, the response voltage waveforms hold diverse forms and patterns due to distinguished initial contact area shape and overall weight distribution of tested objects, which certificated the PENG's dynamic sensitivity of tactile sensing. Dynamic stability and durability of the PENG was evaluated by repetitive continuous pressing-releasing test for over $12,000$ cycles (Fig. 5j).

Owing to the excellent flexibility and intrinsic nanofibrous structure, as shown in Fig. 5j zoomed-in figures, the PENG performs outstanding robustness that no obvious deterioration in output amplitude is observed throughout the load testing cycles, verifying the potential of adopting such PENG as wearable tactile sensor for long-term usage. Overall, the tactile sensing performance of the PENG in terms of sensitivity and device durability has shown advantages when compared with similar reported works, depicted in Fig. S7, and detailed parameters are listed in Table S1.

Nanofibrous PENG as a Health-Care Tactile Sensor

Eventually, we investigated the application of the developed PENG device for healthcare by attaching it on human body as a self-powered motion sensor to harvest mechanical energies of movements. Several sets of actions were designed to exploit the PENG's motion sensing capability which attached to selected spots (elbow, hip, thigh, knee, and ankle) over the body (Fig. 6a). Generated voltage waveforms were inspected at these locations, each performed unique responses in terms of signal duration, intensity span, waveform pattern and complexity. For instance, voltage generated by elbow bending generally falls in the range of below 5 mV (Fig. 6b), where the peaks are followed by modest oscillation, owing to the prolonged timespan of elbow bending-stretching movement. While the voltage harvested from hip with movement of leg lifting (Fig. 6c upper left) has a similar peak amplitude, its oscillation is more gathered around peaks due to the inertia of lifting/dropping movement instead of distributing widely. The voltage peaks occur with a higher frequency during periodic light jumping (Fig. 6c upper right). In the lower section of Fig. 6c, it can be seen that the PENG sensor is able to distinguish motions with different intensity as well. Apparently, difference in walking speed leads to discrepancy in response magnitude that periodic slow walking generates a peak voltage within 4 mV , whereas periodic fast walking generates a peak voltage of $10\text{--}20\text{ mV}$. Since the PENG shows great stability and sensitivity, it reflects the frequency as well as the magnitude external stimuli. Interestingly, when adhering the PENG sensor on thigh (Fig. 6d), diverse patterns can be observed of foot lifting dependent upon the foot separating region. We suspect this to be attributed to the fact that the wearer's body weight distributes in the manner that the center of gravity is slightly deviate towards the heel from the center of heel and forefoot, resulting in a stronger response when lift foot from heel. Excellent sensitivity in lower pressure range ensures the PENG device's ability to react to even the slight deformations. For example, sensor attached on inner ankle tracks respiratory rate with wearer sits in a cross-legged position. It performs a clear decrescendo trend with output voltage from 1.7 to 0.7 mV when the wearer sits down and recovers from movement (Fig. 6f left and middle). After relaxation, the PENG device monitors the minor

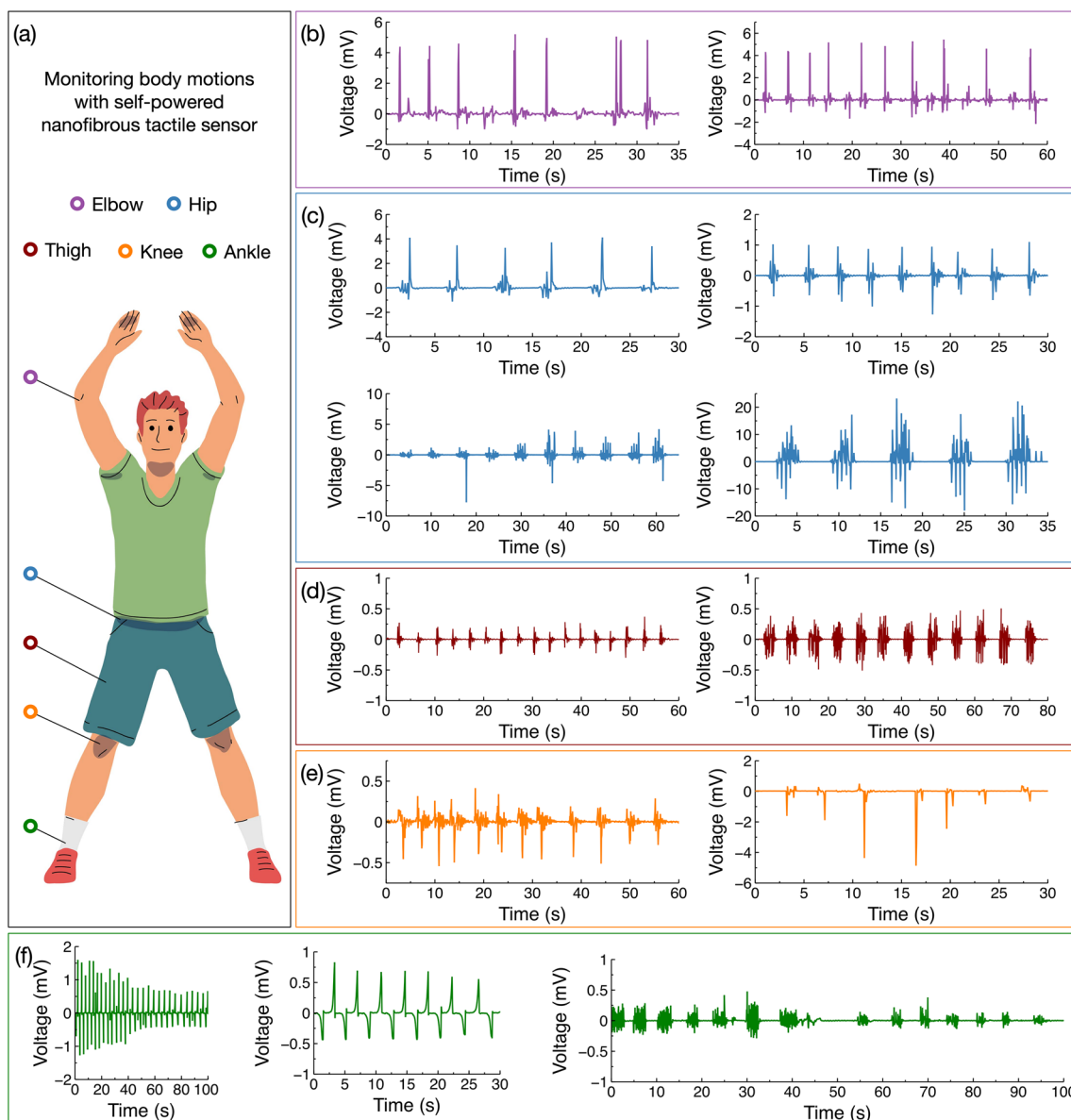


Fig. 6 Body motion detection and recognition using PENG device based on ESNF membrane. **a** Locations of the PENG sensor device attachment and their corresponding waveform responses from: **b** elbow: bending-stretching, **c** hip: periodic leg lifting (up left), periodic jumping (up right), periodic slow walking (lower left) and periodic fast walking (lower right), **d** thigh: forefoot lifting (left)

versus heel lifting (right), **e** knee: leg lifting (left) and bending (right), **f** ankle: tracking respiratory rate of the wearer in relaxing process, heavy breath after movement (left) and normal breath after relaxation (middle), as well as major/minor periodic foot tapping sitting with relaxed state (right)

deformation induced by wear breathing, which shows a normal respiration rate of around 15 times per minute. Surely the device on ankle also responds to other movements when motion range goes up, such as foot tapping where cyclic tapping of 5 times each set every 5 s was exhibited (Fig. 6f right).

All above results verified the feasibility of the PENG device as tactile sensor for human motion monitoring and recognition, implying its potential for exercise tracking and rehabilitation.

Conclusions

A self-powered piezoelectric nanofibrous membrane as wearable tactile sensor was successfully fabricated through electrospinning for human body motion monitoring and recognition. The PVDF-based ESNF membrane's favorable mechanical and electrical properties such as flexibility, durability, hydrophobicity, breathability, and permeability, make it particularly suitable for wearable tactile sensors.

The improved β -phase content in the ESNF membrane also ensures its piezoelectric performance. The assembled PENG sensing device exhibits an outstanding sensitivity over a wide range of pressure ($116\text{mV}\cdot\text{kPa}^{-1}$ in precise pressure detection of 0–10 N, and $6.6\text{mV}\cdot\text{kPa}^{-1}$ for load within 10–100 N), a rapid response time of 82.7 ms, and excellent durability over 12,000 loading test cycles. Furthermore, the PENG device can be used as a wearable tactile sensor, generating representative waveform voltage patterns that correspond to diverse body motions through generating representative waveform voltage patterns. This demonstrates the potential for the PENG tactile sensor to expand the application of self-powered electronic wearables and offer a convenient way of body motion monitoring and recognition. As demonstrated, the PENG tactile sensor enlarges the application of self-powered electronic wearables and offers a feasible and convenient way of body motion monitoring and recognition.

Supplementary Information The online version contains supplementary material available at <https://doi.org/10.1007/s42765-023-00282-8>.

Acknowledgements This work was supported by National Research Foundation (Sustainable Tropical Data Centre Test bed: A-0009465-05-00). L.J.C would like to acknowledge the support from NUS Research Scholarship (GOSU0000042 PVO ARS-FOE 101 IS).

Declarations

Conflict of interest The authors claim no conflicts of interest.

Appendix A. Supplementary data Supplementary data related to this article can be found at [Supplementary Data – a self-powered PENG. pdf].

References

- Lim H-R, Kim HS, Qazi R, Kwon Y-T, Jeong J-W, Yeo W-H. Advanced soft materials, sensor integrations, and applications of wearable flexible hybrid electronics in healthcare, energy, and environment. *Adv Mater*. 2020;32:1901924. <https://doi.org/10.1002/adma.201901924>.
- Xie M, Hisano K, Zhu M, Toyoshi T, Pan M, Okada S, Tsutsumi O, Kawamura S, Bowen C. Flexible multifunctional sensors for wearable and robotic applications. *Adv Mater Technol*. 2019;4:1800626. <https://doi.org/10.1002/admt.201800626>.
- Zeng W, Shu L, Li Q, Chen S, Wang F, Tao X-M. Fiber-based wearable electronics: a review of materials, fabrication, devices, and applications. *Adv Mater*. 2014;26:5310–36. <https://doi.org/10.1002/adma.201400633>.
- Zhang Y, Wang H, Lu H, Li S, Zhang Y. Electronic fibers and textiles: recent progress and perspective. *IScience*. 2021. <https://doi.org/10.1016/j.isci.2021.102716>.
- Li J, Yin J, Ramakrishna S, Ji D. Smart mask as wearable for post-pandemic personal healthcare. *Biosensors*. 2023;13:205. <https://doi.org/10.3390/bios13020205>.
- Ni QQ, Guan X, Zhu Y, Dong Y, Xia H. Nanofiber-based wearable energy harvesters in different body motions. *Compos Sci Technol*. 2020;200:108478–8. <https://doi.org/10.1016/j.compscitech.2020.108478>.
- Gao S, He T, Zhang Z, Ao H, Jiang H, Lee C. Capturing and energy harvesting hybridized lower-limb system for rehabilitation and sports applications. *Adv Sci*. 2021. <https://doi.org/10.1002/advs.202101834>.
- Kim KK, Ha I, Kim M, Choi J, Won P, Jo S, Ko SH. A deep-learned skin sensor decoding the epicentral human motions. *Nat Commun*. 2020;11:2149. <https://doi.org/10.1038/s41467-020-16040-y>.
- Khandelwal G, Maria Joseph Raj NP, Kim S-J. Triboelectric nanogenerator for healthcare and biomedical applications. *Nano Today*. 2020;33:100882. <https://doi.org/10.1016/j.nantod.2020.100882>.
- Luo J, Gao W, Wang ZL. The triboelectric nanogenerator as an innovative technology toward intelligent sports. *Adv Mater*. 2021;33:2004178. <https://doi.org/10.1002/adma.202004178>.
- Zhang S, Zhang B, Zhang J, Ren K. Enhanced piezoelectric performance of various electrospun PVDF nanofibers and related self-powered device applications. *ACS Appl Mater Interfaces*. 2021;13:32242–50. <https://doi.org/10.1021/acsami.1c07995>.
- Yang T, Pan H, Tian G, Zhang B, Xiong D, Gao Y, Yan C, Chu X, Chen N, Zhong S, Zhang L, Deng W, Yang W. Hierarchically structured PVDF/ZnO core-shell nanofibers for self-powered physiological monitoring electronics. *Nano Energy*. 2020;72:104706. <https://doi.org/10.1016/j.nanoen.2020.104706>.
- Maity K, Garain S, Henkel K, Schmeißer D, Mandal D. Self-powered human-health monitoring through aligned PVDF nanofibers interfaced skin-interactive piezoelectric sensor. *ACS Appl Polym Mater*. 2020;2:862–78. <https://doi.org/10.1021/acsapm.9b00846>.
- Zhu C, Wu J, Yan J, Liu X. Advanced fiber materials for wearable electronics. *Adv Fiber Mater*. 2023;5:12–35. <https://doi.org/10.1007/s42765-022-00212-0>.
- Wu Y, Bakker E. Self-powered signal transduction of ion-selective electrodes to an electronic paper display. *ACS Sens*. 2022;7:3201–7. <https://doi.org/10.1021/acssensors.2c01826>.
- Li Q, Xu Y, Qi J, Zheng X, Liu S, Lin D, Zhang L, Liu P, Li B, Chen L. A self-powered rotating paper-based analytical device for sensing of thrombin. *Sens Actuators B*. 2022;351:130917. <https://doi.org/10.1016/j.snb.2021.130917>.
- Eun JH, Sung SM, Kim MS, Choi BK, Lee JS. Effect of MWCNT content on the mechanical and piezoelectric properties of PVDF nanofibers. *Mater Design*. 2021;206:109785. <https://doi.org/10.1016/j.matdes.2021.109785>.
- Jingcheng L, Reddy VS, a W, Jayathilaka DM, Chinnappan A, Ramakrishna S, Ghosh R. Intelligent polymers, fibers and applications. *Polymers*. 2021;13:1427. <https://doi.org/10.3390/polym13091427>.
- Wang X, Sun F, Yin G, Wang Y, Liu B, Dong M. Tactile-sensing based on flexible PVDF nanofibers via electrospinning: a review. *Sens (Switzerland)*. 2018. <https://doi.org/10.3390/s18020330>.
- Syu MH, Guan YJ, Lo WC, Fuh YK. Biomimetic and porous nanofiber-based hybrid sensor for multifunctional pressure sensing and human gesture identification via deep learning method. *Nano Energy*. 2020;76:105029–9. <https://doi.org/10.1016/j.nanoen.2020.105029>.
- Li X, Ji D, Yu B, Ghosh R, He J, Qin X, Ramakrishna S. Boosting piezoelectric and triboelectric effects of PVDF nanofiber through carbon-coated piezoelectric nanoparticles for highly sensitive wearable sensors. *Chem Eng J*. 2021;426:130345. <https://doi.org/10.1016/j.cej.2021.130345>.
- Zhou Z, Du X, Luo J, Yao L, Zhang Z, Yang H, Zhang Q. Coupling of interface effects and porous microstructures in translucent piezoelectric composites for enhanced energy harvesting and sensing. *Nano Energy*. 2021;84:105895–5. <https://doi.org/10.1016/j.nanoen.2021.105895>.

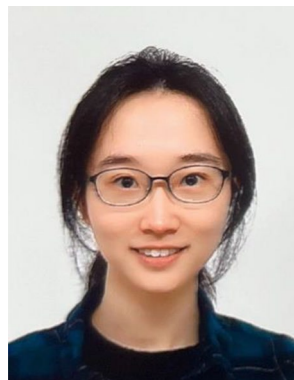
23. You M-H, Wang X-X, Yan X, Zhang J, Song W-Z, Yu M, Fan Z-Y, Ramakrishna S, Long Y-Z. A self-powered flexible hybrid piezoelectric–pyroelectric nanogenerator based on non-woven nanofiber membranes. *J Mater Chem A*. **2018**;6:3500–9. <https://doi.org/10.1039/C7TA10175A>.
24. Lang C, Fang J, Shao H, Ding X, Lin T. High-sensitivity acoustic sensors from nanofibre webs. *Nat Commun*. **2016**;7:11108. <https://doi.org/10.1038/ncomms11108>.
25. Tian G, Deng W, Gao Y, Xiong D, Yan C, He X, Yang T, Jin L, Chu X, Zhang H, Yan W, Yang W. Rich lamellar crystal baklava-structured PZT/PVDF piezoelectric sensor toward individual table tennis training. *Nano Energy*. **2019**;59:574–81. <https://doi.org/10.1016/j.nanoen.2019.03.013>.
26. Houis S, Engelhardt EM, Wurm F, Gries T. Application of polyvinylidene fluoride (PVDF) as a biomaterial in medical textiles, In: S.C. Anand, J.F. Kennedy, M. Miraftab, S. Rajendran, (eds), Medical and healthcare textiles, Woodhead Publishing, **2010**: pp. 342–352. <https://doi.org/10.1533/9780857090348.342>.
27. Panda S, Hajra S, Jeong H, Panigrahi BK, Pakawanit P, Dubal D, Hong S, Kim HJ. Biocompatible CaTiO₃-PVDF composite-based piezoelectric nanogenerator for exercise evaluation and energy harvesting. *Nano Energy*. **2022**;102:107682. <https://doi.org/10.1016/j.nanoen.2022.107682>.
28. He Z, Rault F, Lewandowski M, Mohsenzadeh E, Salaün F. Electrospun PVDF nanofibers for piezoelectric applications: a review of the influence of electrospinning parameters on the β phase and crystallinity enhancement. *Polymers*. **2021**;13:174. <https://doi.org/10.3390/polym13020174>.
29. Al-Dhahebi AM, Ling J, Krishnan SG, Yousefzadeh M, Elumalai NK, Saheed MSM, Ramakrishna S, Jose R. Electrospinning research and products: the road and the way forward. *Appl Phys Rev*. **2022**;9:011319. <https://doi.org/10.1063/5.0077959>.
30. Adedoyin AA, Ekenseair AK. Biomedical applications of magneto-responsive scaffolds. *Nano Res*. **2018**;11:5049–64. <https://doi.org/10.1007/s12274-018-2198-2>.
31. He J, Jiang N, Qin T, Zhang W, Liu Z, Liu Y, Li D. Microfiber-reinforced nanofibrous scaffolds with structural and material gradients to mimic ligament-to-bone interface. *J Mater Chem B*. **2017**;5:8579–90. <https://doi.org/10.1039/C7TB02089A>.
32. Deng Y, Lu T, Cui J, Keshari Samal S, Xiong R, Huang C. Bio-based electrospun nanofiber as building blocks for a novel eco-friendly air filtration membrane: a review. *Sep Purif Technol*. **2021**. <https://doi.org/10.1016/j.seppur.2021.119623>.
33. Li M, Li J, Zhou M, Xian Y, Shui Y, Wu M, Yao Y. Super-hydrophilic electrospun PVDF/PVA-blended nanofiber membrane for microfiltration with ultrahigh water flux. *J Appl Polym Sci*. **2020**;137:48416. <https://doi.org/10.1002/app.48416>.
34. Castkova K, Kastyl J, Sobola D, Petrus J, Stastna E, Riha D, Tofel P. Structure–properties relationship of electrospun PVDF fibers. *Nanomaterials*. **2020**;10:1221. <https://doi.org/10.3390/nano10061221>.
35. Song Y, Bao J, Hu Y, Cai H, Xiong C, Yang Q, Tian H, Shi Z. Forward polarization enhanced all-polymer based sustainable triboelectric nanogenerator from oriented electrospinning PVDF/cellulose nanofibers for energy harvesting. *Sustainable Energy Fuels*. **2022**;6:2377–86. <https://doi.org/10.1039/D2SE00321J>.
36. Kim M, Fan J. Piezoelectric properties of three types of PVDF and ZnO nanofibrous composites. *Adv Fiber Mater*. **2021**;3:160–71. <https://doi.org/10.1007/s42765-021-00068-w>.
37. Xue L, Fan W, Yu Y, Dong K, Liu C, Sun Y, Zhang C, Chen W, Lei R, Rong K, Wang Q. A novel strategy to fabricate core-sheath structure piezoelectric yarns for wearable energy harvesters. *Adv Fiber Mater*. **2021**;3:239–50. <https://doi.org/10.1007/s42765-021-00081-z>.
38. Park SC, Nam C, Baek C, Lee M-K, Lee G-J, Park K-I. Enhanced piezoelectric performance of composite fibers based on lead-free BCTZ ceramics and P(VDF-TrFE) piezopolymer for self-powered wearable sensors. *ACS Sustainable Chem Eng*. **2022**;10:14370–80. <https://doi.org/10.1021/acssuschemeng.2c05026>.
39. Doshi J, Reneker DH. Electrospinning process and applications of electrospun fibers. *J Electrostat*. **1995**;35:151–60. [https://doi.org/10.1016/0304-3886\(95\)00041-8](https://doi.org/10.1016/0304-3886(95)00041-8).
40. Cozza ES, Monticelli O, Marsano E, Cebe P. On the electrospinning of PVDF: influence of the experimental conditions on the nanofiber properties. *Polym Int*. **2013**;62:41–8. <https://doi.org/10.1002/pi.4314>.
41. Liu Z, Li S, Zhu J, Mi L, Zheng G. Fabrication of β -phase-enriched PVDF sheets for self-powered piezoelectric sensing. *ACS Appl Mater Interfaces*. **2022**;14:11854–63. <https://doi.org/10.1021/acami.2c01611>.
42. Yousry YM, Yao K, Chen S, Liew WH, Ramakrishna S. Mechanisms for enhancing polarization orientation and piezoelectric parameters of PVDF nanofibers. *Adv Electron Mater*. **2018**;4:1700562. <https://doi.org/10.1002/aelm.201700562>.
43. Zueva OS, Makshakova ON, Idiyatullin BZ, Faizullin DA, Benevolenskaya NN, Borovskaya AO, Sharipova EA, Osin YuN, Salnikov VV, Zuev YuF. Structure and properties of aqueous dispersions of sodium dodecyl sulfate with carbon nanotubes. *Russ Chem Bull*. **2016**;65:1208–15. <https://doi.org/10.1007/s11172-016-1437-5>.
44. Kharisov BI, Kharissova OV, Méndez UO. Methods for dispersion of carbon nanotubes in water and common solvents. *MRS Online Proc Library*. **2014**;1700:109–14. <https://doi.org/10.1557/opl.2014.605>.
45. Jayathilaka WADM, Chinnappan A, Ji D, Ghosh R, Tran TQ, Ramakrishna S. Facile and scalable electrospun nanofiber-based alternative current electroluminescence (ACEL) device. *ACS Appl Electron Mater*. **2021**;3:267–76. <https://doi.org/10.1021/acsaelm.0c00838>.
46. Tsangaris GM, Psarras GC, Tsangaris GM. Electric modulus and interfacial polarization in composite polymeric systems. *J Mater Sci*. **1998**;33:2027–37. <https://doi.org/10.1023/A:1004398514901>.
47. Sharma M, Srinivas V, Madras G, Bose S. Outstanding dielectric constant and piezoelectric coefficient in electrospun nanofiber mats of PVDF containing silver decorated multiwall carbon nanotubes: assessing through piezoresponse force microscopy. *RSC Adv*. **2016**;6:6251–8. <https://doi.org/10.1039/C5RA25671B>.
48. Huang A, Liu F, Cui Z, Wang H, Song X, Geng L, Wang H, Peng X. Novel PTFE/CNT composite nanofiber membranes with enhanced mechanical, crystalline, conductive, and dielectric properties fabricated by emulsion electrospinning and sintering. *Compos Sci Technol*. **2021**;214:108980. <https://doi.org/10.1016/j.compscitech.2021.108980>.
49. Gregorio R, Ueno EM. Effect of crystalline phase, orientation and temperature on the dielectric properties of poly (vinylidene fluoride) (PVDF). *J Mater Sci*. **1999**;34:4489–500. <https://doi.org/10.1023/A:1004689205706>.
50. Thakur Y, Zhang T, Jacob C, Yang T, Bernholc J, Chen LQ, Runt J, Zhang QM. Enhancement of the dielectric response in polymer nanocomposites with low dielectric constant fillers. *Nanoscale*. **2017**;9:10992–7. <https://doi.org/10.1039/C7NR01932G>.
51. Liu S, Xue S, Zhang W, Zhai J, Chen G. Significantly enhanced dielectric property in PVDF nanocomposites flexible films through a small loading of surface-hydroxylated Ba_{0.6}Sr_{0.4}TiO₃ nanotubes. *J Mater Chem A*. **2014**;2:18040–6. <https://doi.org/10.1039/C4TA04051A>.
52. Sharma M, Madras G, Bose S. Process induced electroactive β -polymorph in PVDF: effect on dielectric and ferroelectric properties. *Phys Chem Chem Phys*. **2014**;16:14792. <https://doi.org/10.1039/c4cp01004c>.
53. Chi Q, Ma T, Zhang Y, Chen Q, Zhang C, Cui Y, Zhang T, Lin J, Wang X, Lei Q. Excellent energy storage of sandwich-structured

- PVDF-Based composite at Low Electric Field by introduction of the hybrid CoFe_2O_4 @BZT–BCT nanofibers. *ACS Sustainable Chem Eng.* **2018**;6:403–12. <https://doi.org/10.1021/acssuschemeng.7b02659>.
54. Lu X, Peng Y, Qiu H, Liu X, Ge L. Anti-fouling membranes by manipulating surface wettability and their anti-fouling mechanism. *Desalination.* **2017**;413:127–35. <https://doi.org/10.1016/j.desal.2017.02.022>.
 55. Kim M, Wu YS, Kan EC, Fan J. Breathable and flexible piezoelectric ZnO@PVDF fibrous nanogenerator for wearable applications. *Polymers.* **2018**;10:745. <https://doi.org/10.3390/polym10070745>.
 56. Jiang G, Luo L, Tan L, Wang J, Zhang S, Zhang F, Jin J. Microsphere-fiber interpenetrated superhydrophobic PVDF microporous membranes with improved waterproof and breathable performance. *ACS Appl Mater Interfaces.* **2018**;10:28210–8. <https://doi.org/10.1021/acsami.8b08191>.
 57. Yue Y, Gong X, Jiao W, Li Y, Yin X, Si Y, Yu J, Ding B. In-situ electrospinning of thymol-loaded polyurethane fibrous membranes for waterproof, breathable, and antibacterial wound dressing application. *J Colloid Interface Sci.* **2021**;592:310–8. <https://doi.org/10.1016/j.jcis.2021.02.048>.
 58. Nishiyama T, Sumihara T, Sasaki Y, Sato E, Yamato M, Horibe H. Crystalline structure control of poly(vinylidene fluoride) films with the antisolvent addition method. *Polym J.* **2016**;48:1035–8. <https://doi.org/10.1038/pj.2016.62>.
 59. Cai X, Lei T, Sun D, Lin L. A critical analysis of the α , β and γ phases in poly(vinylidene fluoride) using FTIR. *RSC Adv.* **2017**;7:15382–9. <https://doi.org/10.1039/C7RA01267E>.
 60. Salimi A, Yousefi AA, Method A. FTIR studies of β -phase crystal formation in stretched PVDF films. *Polym Test.* **2003**;22:699–704. [https://doi.org/10.1016/S0142-9418\(03\)00003-5](https://doi.org/10.1016/S0142-9418(03)00003-5).
 61. Yee WA, Kotaki M, Liu Y, Lu X. Morphology, polymorphism behavior and molecular orientation of electrospun poly(vinylidene fluoride) fibers. *Polymer.* **2007**;48:512–21. <https://doi.org/10.1016/j.polymer.2006.11.036>.
 62. Yu S, Zheng W, Yu W, Zhang Y, Jiang Q, Zhao Z. Formation mechanism of β -phase in PVDF/CNT composite prepared by the sonication method. *Macromolecules.* **2009**;42:8870–4. <https://doi.org/10.1021/ma901765j>.
 63. Ruan L, Yao X, Chang Y, Zhou L, Qin G, Zhang X. Properties and applications of the β phase poly(vinylidene fluoride). *Polymers.* **2018**;10:228. <https://doi.org/10.3390/polym10030228>.
 64. Wan C, Bowen CR. Multiscale-structuring of polyvinylidene fluoride for energy harvesting: the impact of molecular-, micro- and macro-structure. *J Mater Chem A.* **2017**;5:3091–128. <https://doi.org/10.1039/C6TA09590A>.
 65. Wang Y, Yeow JTW. A review of carbon nanotubes-based gas sensors. *J Sens.* **2009**. <https://doi.org/10.1155/2009/493904>.
 66. Zhao B, Chen Z, Cheng Z, Wang S, Yu T, Yang W, Li Y. Piezoelectric nanogenerators based on electrospun PVDF-coated mats composed of multilayer polymer-coated BaTiO_3 nanowires. *ACS Appl Nano Mater.* **2022**. <https://doi.org/10.1021/acsanm.2c01538>.
 67. Martins P, Lopes AC, Lanceros-Mendez S. Electroactive phases of poly(vinylidene fluoride): determination, processing and applications. *Prog Polym Sci.* **2014**;39:683–706. <https://doi.org/10.1016/j.progpolymsci.2013.07.006>.
 68. Lolla D, Gorse J, Kisielowski C, Miao J, Taylor PL, Chase GG, Reneker DH. Polyvinylidene fluoride molecules in nanofibers, imaged at atomic scale by aberration corrected electron microscopy. *Nanoscale.* **2016**;8:120–8. <https://doi.org/10.1039/C5NR01619C>.
 69. Lee J-H, Lee KY, Gupta MK, Kim TY, Lee D-Y, Oh J, Ryu C, Yoo WJ, Kang C-Y, Yoon S-J, Yoo J-B, Kim S-W. Highly stretchable piezoelectric-pyroelectric hybrid nanogenerator. *Adv Mater.* **2014**;26:765–9. <https://doi.org/10.1002/adma.201303570>.

70. Askari H, Xu N, Groenner Barbosa BH, Huang Y, Chen L, Khajepour A, Chen H, Wang ZL. Intelligent systems using triboelectric, piezoelectric, and pyroelectric nanogenerators. *Mater Today.* **2022**. <https://doi.org/10.1016/j.mattod.2021.11.027>.

Publisher's Note Springer Nature remains neutral with regard to jurisdictional claims in published maps and institutional affiliations.

Springer Nature or its licensor (e.g. a society or other partner) holds exclusive rights to this article under a publishing agreement with the author(s) or other rightsholder(s); author self-archiving of the accepted manuscript version of this article is solely governed by the terms of such publishing agreement and applicable law.



Jingcheng Li is currently a Ph.D. candidate at National University of Singapore (NUS). Her research focuses on the development of tactile sensors using nanofibers, with a specific emphasis on piezoelectrics. She also investigates the potential of utilizing AI-powered intelligent materials for healthcare devices.



Jing Yin is a Ph.D. student in Soochow University, China. She is also an exchange Ph.D. student in National University of Singapore. Her research interests include the development on the new electrospinning device, the numerical simulation of the spinning process, and smart textile.



Mei Gui Vanessa Wee graduated from the National University of Singapore (NUS) in 2019 with a Bachelor of Science (Chemistry) with Honors (Highest Distinction). She has previously worked at a local start-up, Tech Trove, to develop handheld gas sensors. Currently, as part of her Ph.D., she is working with Prof. Seeram Ramakrishna and Dr. Amutha Chinappan at NUS on desiccant-coated heat exchangers for a tropical data center testbed. Her fields of interest include environmental chemistry, materials science, product research, and product design.

ence, product research, and product design.



Dr Amutha Chinnappan received her Ph.D. degree in organic nanomaterials using ionic liquids for energy applications from Myongji University, South Korea in 2013. She then worked as a BK21 Postdoctoral Fellow until 2015, and after that became an Assistant Professor (Research) at the Department of Energy, Science and Technology, Myongji University. She is currently working as a Senior Research Fellow at the Center for Nanofibers & Nanotechnology, National University of Singapore. Her

current research interests include green chemistry, circular economy/sustainability, plastic recycling, conducting cables/ wires, smart textiles, wearable/flexible electronics, and ionic liquid-based functional nanomaterials for energy applications.



Seeram Ramakrishna is a world-renowned poly-disciplinary scholar at the National University of Singapore. He is named among the World's Most Influential Minds (Thomson Reuters); and Top 1% Highly Cited Researchers in material science as well as cross-field categories (Clarivate Analytics). His publications to date have an H-index of 177 and over 151,637 citations. He is an elected Fellow of UK Royal Academy of Engineering (FREng); AAAS; ASM International; ASME; and

AIMBE, USA. He is an Editorial board member of RSC Energy and Environmental Science journal, NPJ Urban Sustainability journal; eScience journal, and Advanced Fiber Materials journal.